

CARMA MEASUREMENTS OF THE SUNYAEV-ZEL'DOVICH EFFECT IN RX J1347.5–1145

THOMAS J. PLAGGE,¹ DANIEL P. MARRONE,^{1,2} ZUBAIR ABDULLA,¹ MASSIMILIANO BONAMENTE,^{3,4} JOHN E. CARLSTROM,^{1,5,6}
MEGAN GRALLA,^{1,7} CHRISTOPHER H. GREER,¹ MARSHALL JOY,⁴ JAMES W. LAMB,⁸ ERIK M. LEITCH,¹ ADAM MANTZ,¹
STEPHEN MUCHOJEJ,⁸ AND DAVID WOODY⁸

Draft version May 10, 2021

ABSTRACT

We demonstrate the Sunyaev-Zel'dovich (SZ) effect imaging capabilities of the Combined Array for Research in Millimeter-wave Astronomy (CARMA) by presenting an SZ map of the galaxy cluster RX J1347.5–1145. By combining data from multiple CARMA bands and configurations, we are able to capture the structure of this cluster over a wide range of angular scales, from its bulk properties to its core morphology. We find that roughly 9% of this cluster's thermal energy is associated with sub-arcminute-scale structure imparted by a merger, illustrating the value of high-resolution SZ measurements for pursuing cluster astrophysics and for understanding the scatter in SZ scaling relations. We also find that the cluster's SZ signal is lower in amplitude than suggested by a spherically-symmetric model derived from X-ray data, consistent with compression along the line of sight relative to the plane of the sky. Finally, we discuss the impact of upgrades currently in progress that will further enhance CARMA's power as an SZ imaging instrument.

Subject headings: galaxies: clusters: general

1. INTRODUCTION

Galaxy clusters are the largest gravitationally bound systems in the universe, and have taken nearly a Hubble time to form. They therefore have the potential to act as powerful probes of cosmology if systematic errors can be controlled. Precision cluster cosmology will require a deep understanding of cluster astrophysics, particularly as it relates to the hot gas of the intracluster medium (ICM). The most detailed studies of the ICM have thus far been performed by X-ray telescopes, which are sensitive to the bremsstrahlung emission from the 10^7 – 10^8 K gas. The Sunyaev-Zel'dovich (SZ) effect is a complementary probe of the ICM. The amplitude of the SZ signal depends on the line-of-sight integral of $n_e T$, while the X-ray surface brightness depends on n_e^2 , so sensitive SZ measurements can access tenuous gas outside the cluster core and directly measure pressure disturbances. Features found commonly in the outer regions of clusters, such as shocked gas from mergers, may therefore be easier to detect using the SZ effect than using X-rays. Moreover, the combination of X-ray and SZ data can be used to obtain a more complete picture of the ICM thermodynamics.

To take advantage of these opportunities, advances in

SZ imaging capabilities are needed. Measurements of the SZ effect have become routine over the last decade, but the full potential of the SZ effect as a probe of cluster physics remains largely unexploited due to technical challenges: the combination of high sensitivity and large angular dynamic range required for detailed SZ imaging has proven difficult to achieve with existing instruments. As a result, the use of the SZ effect has been limited primarily to studies where resolved imaging is unnecessary.

The small number of higher-resolution SZ images obtained to date have served to demonstrate the utility of the technique. However, single-dish measurements such as those by Korngut et al. (2011) can suffer from radio point source contamination and have been limited to scales $< 45''$ by the necessity of filtering out modes contaminated by atmospheric noise. Multi-dish SZ measurements by arrays such as ATCA (e.g., Malu et al. 2010) can constrain and remove point sources using the inherent spatial filtering ability of interferometers, but most millimeter-wave interferometers lack sensitivity at arcminute angular scales where the SZ cluster signal is largest.

CARMA is a heterogeneous interferometric array consisting of 23 antennas with diameters of 3.5, 6.1, and 10.4 m operating at 1 cm, 3 mm, and 1 mm. This particular combination of antennas and bands makes CARMA a uniquely powerful SZ instrument: its 3.5 m antennas can be placed in a compact configuration sensitive to arcminute-scale emission, and its 6.1 and 10.4 m dishes can be used to obtain the sensitivity necessary to resolve smaller angular scale SZ features. In this work, we make use of CARMA data from three array configurations and two bands to obtain an SZ image of the galaxy cluster RX J1347.5–1145. These data represent the highest-fidelity picture of a galaxy cluster ever obtained using the SZ effect.

This paper is organized as follows: Section 2 provides background on RX J1347.5–1145, Section 3 describes the observations and data reduction, and Section 4 discusses

¹ Kavli Institute for Cosmological Physics, Department of Astronomy and Astrophysics, University of Chicago, Chicago, IL 60637, USA

² Steward Observatory, University of Arizona, 933 North Cherry Avenue, Tucson, AZ 85721, USA

³ Department of Physics, University of Alabama, Huntsville, AL 35899, USA

⁴ Space Science-VP62, NASA Marshall Space Flight Center, Huntsville, AL 35812, USA

⁵ Enrico Fermi Institute, University of Chicago, Chicago, IL 60637, USA

⁶ Department of Physics, University of Chicago, Chicago, IL 60637, USA

⁷ Department of Physics and Astronomy, Johns Hopkins University, Baltimore, MD 21218, USA

⁸ Owens Valley Radio Observatory, California Institute of Technology, Big Pine, CA 93513, USA

the modeling and deconvolution method. We present our results and compare them to previous measurements in Section 5, and review the conclusions and discuss prospects for future work in Section 6.

2. RX J1347.5–1145

The target for these observations is the cluster RX J1347.5–1145, an object that has been characterized extensively using a variety of techniques. First discovered by the ROSAT all-sky survey (Voges et al. 1999), RX J1347.5–1145 is the most luminous cluster known in the X-ray sky, and has been measured by several X-ray instruments including *Chandra* (Allen et al. 2002) and *XMM-Newton* (Gitti & Schindler 2004). Optical observations have revealed the presence of two cD galaxies, one coincident with the X-ray emission peak and one directly to the east. The system has also been found to host a radio mini-halo (Gitti et al. 2007). Its gravitational potential has been probed using both strong and weak gravitational lensing (e.g., Miranda et al. 2008; Bradač et al. 2008). These multi-wavelength observations indicate that RX J1347.5–1145 is a massive ($> 10^{15} M_{\odot}$) cluster at redshift $z = 0.4510$ which has recently undergone a merger with a smaller object. The cluster’s SZ signal has been measured using single-dish (Komatsu et al. 2000; Kitayama et al. 2004; Korngut et al. 2011) and interferometric (Carlstrom et al. 2002; Bonamente et al. 2008, 2011) imaging instruments, and its spectrum near the thermal SZ null has also been characterized (Zemcov et al. 2012). The higher angular resolution measurements have revealed a compact region of very hot (~ 20 keV) gas to the southeast of the X-ray emission peak, while the low-resolution data indicate a smaller arcminute-scale SZ signal than suggested by a spherical fit to the X-ray data.

The existence of a central radio-bright AGN, along with the limited angular dynamic range of most SZ instruments, has complicated efforts to bring SZ data to bear on understanding this system. The CARMA data we present help to overcome both limitations.

3. OBSERVATIONS AND DATA REDUCTION

RX J1347.5–1145 was observed with three different sets of CARMA antennas at two wavelengths: an 8-element sub-array consisting of 3.5 m antennas at 1 cm (“CARMA-8”), a 15-element sub-array consisting of 6.1 m and 10.4 m antennas at 3 mm (“CARMA-15”), and the full 23-element array at 3 mm (“CARMA-23”).

The CARMA-8 data were obtained in August 2009 and totaled 25.7 hours of unflagged, on-source time. The center frequency was 31 GHz with a bandwidth of 8 GHz, and the target R.A. and decl. were 13:47:30.7 and -11:45:08.6 in J2000 coordinates. The array was configured with six elements in a compact array sensitive to arcminute-scale SZ signals, and two outlying elements providing simultaneous discrimination for compact radio source emission. The compact array and longer baselines sample uv -spacings of $350\text{--}1300 \lambda$ and $2\text{--}7.5 k\lambda$, respectively. The data were reduced using the Sunyaev-Zel’dovich Array (SZA) pipeline described in Muchovjev et al. (2007).

The CARMA-15 data were obtained in July 2010 and totaled 7.4 hours of unflagged, on-source time. The center frequency was 90 GHz with a bandwidth of 8 GHz, and the target R.A. and decl. were 13:47:32.0

and -11:45:42.0 in J2000 coordinates. The CARMA-15 array was pointed slightly southeast of the CARMA-8 phase center, directly toward the region of hot gas. The antennas were in the E configuration, the most compact standard positions for the 6.1 and 10.4 m antennas. Data reduction was performed using MIRIAD (Sault et al. 1995).

We obtained CARMA-23 data as part of a commissioning run in February 2011. All 23 antennas were operated at a center frequency of 86 GHz and were attached to the CARMA spectral line correlator, which operated at a reduced bandwidth—4 GHz for the double-sideband receivers on the 10.4 and 6.1 m antennas, and 2 GHz for the single-sideband receivers on the 3.5 m antennas. A total of 8.6 hours of unflagged on-source data were obtained; a relatively high fraction of the 3.5 m data were flagged due to hardware issues in the commissioning run that have since been corrected. The target R.A. and decl. were the same as for the CARMA-8 data, and the array configuration was approximately the combined CARMA-8 and CARMA-15 configurations. As with the CARMA-15 data, we reduced the CARMA-23 data using MIRIAD.

For the CARMA-15 and CARMA-23 arrays, we treat each baseline type (10.4m \times 10.4m, 10.4m \times 6.1m, etc.) separately to properly account for the differing primary beams. We therefore have ten data sets: one for CARMA-8, three for CARMA-15, and six for CARMA-23. We apply a cutoff in uv radius for each data set, using the data beyond the cutoff only to constrain the point source emission. The cutoff is chosen to exclude portions of the uv plane which are poorly sampled for a given baseline type.

The outputs of the data reduction pipelines consist of flagged, calibrated visibilities $V(u, v)$. All absolute flux calibration is performed using the Rudy (1987) Mars model, and is accurate to 5%. To combine data from different bands, we define $y(u, v)$, the Fourier-space counterpart to the Compton y parameter (Carlstrom et al. 2002):

$$y(u, v) \equiv \frac{V_{\nu}(u, v)}{g(\nu, \langle T_e \rangle) I_0} \quad (1)$$

where $\langle T_e \rangle = 12$ keV is the mean ICM electron temperature of the cluster⁹. Our ten $y(u, v)$ data sets are summarized in Table 1.

The data weight distribution in the uv plane for the combined data sets is shown in Figure 1. To illustrate the contributions of each of the three sub-arrays, we show the measured $y(u, v)$ binned in uv radius in Figure 2. CARMA-8 at 1 cm constrains the cluster at small uv radius (large angular scale) where the signal is largest, while CARMA-15 and CARMA-23 at 3 mm are sensitive to the large uv radius (small angular scale) substructure of the cluster.

4. MODELING AND DECONVOLUTION

We wish to combine the information in all ten sets of visibility data to form a single image of the cluster. The first step in this process is to remove the radio point

⁹ We make this approximation due to our incomplete knowledge of the true $T_e(x, y, z)$. The relative value of $g(\nu, T_e)$ between 1 cm and 3 mm is nearly independent of T_e , varying by just 2% between 5 and 15 keV.

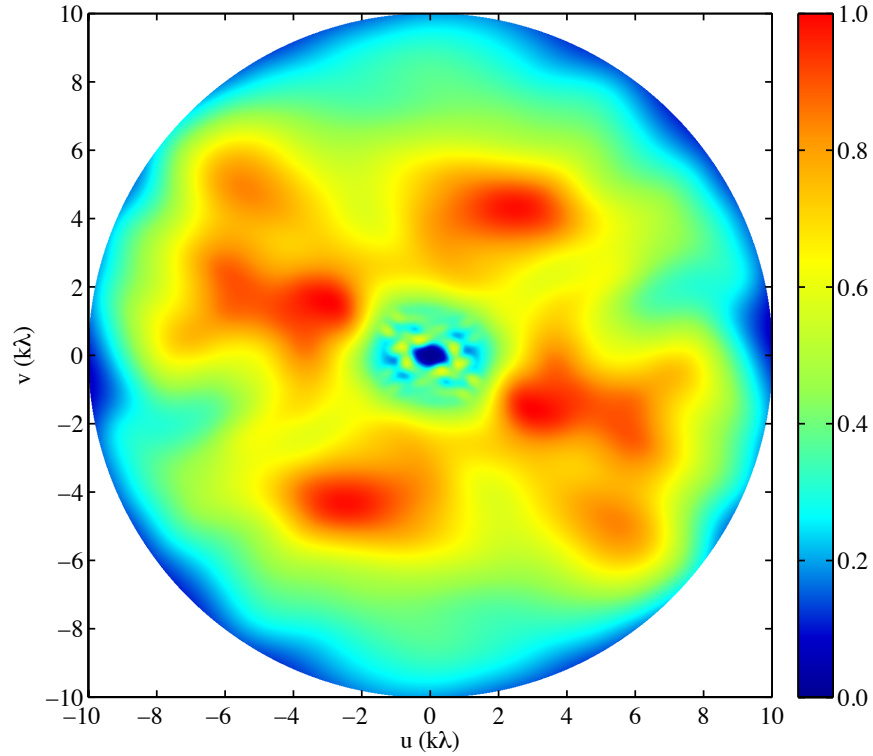


FIG. 1.— Normalized data weight distribution in the uv plane for the union of data sets described in Table 1. Weights are calculated from the inverse variance of each visibility, scaled by the SZ intensity spectrum. The uv -plane extent of each visibility weight is determined from the cross-correlation of the illumination patterns of the corresponding antennas, providing a more complete view of the uv sampling in the heterogeneous array. The weights are well-matched to the cluster signal—which is largest at small uv radius—except for a relatively under-sampled region around $\sim 2 \text{ k}\lambda$. This region of the uv plane will be well-measured by the 23-element CARMA array at 1 cm, which is currently under development.

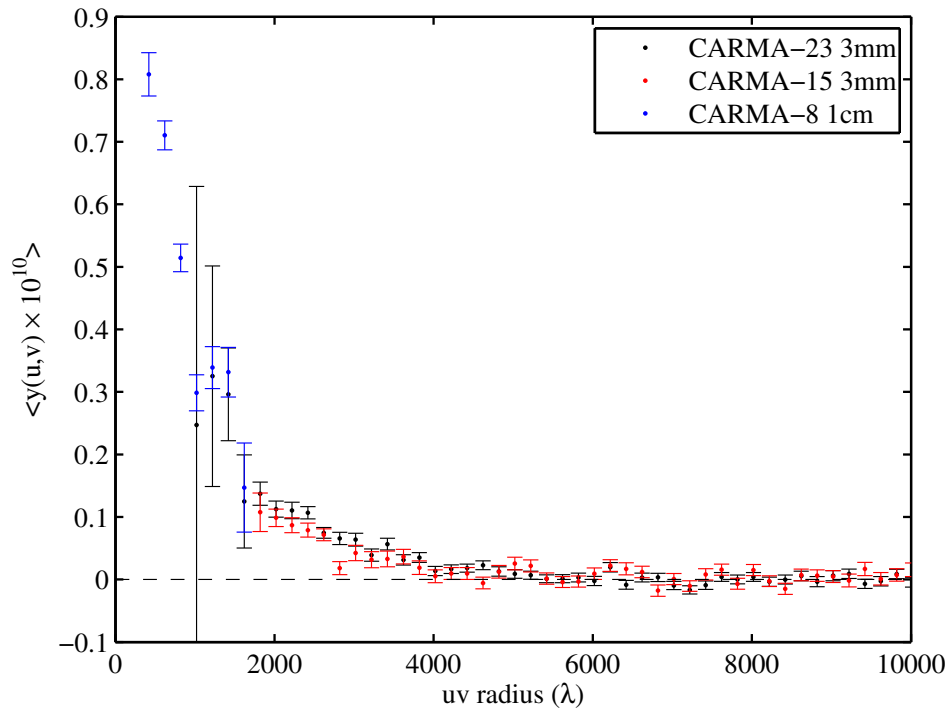


FIG. 2.— Radially binned visibilities from CARMA-8 at 1 cm, CARMA-15 at 3 mm, and CARMA-23 at 3 mm. The CARMA-8 data measure the cluster signal at large angular scales, while the other sub-arrays measure the smaller substructure of the cluster.

source emission, which is accomplished by fitting a point source model to the visibilities above the uv cutoff. Since radio source fluxes often vary considerably with time, identical fluxes should not be expected in the CARMA-15 and CARMA-23 despite their similar central frequencies. We therefore demand consistency within each individual sub-array, but allow the source flux to vary between sub-arrays. We find a best-fit centroid consistent with a source in the NVSS catalog (Condon et al. 1998) at an R.A. and decl. of 13:47:30.7 and -11:45:08.6. The flux of this source was found to be 8.9 ± 0.5 mJy in the 1 cm CARMA-8 data, 4.2 ± 0.2 mJy in the 3 mm CARMA-23 data, and 4.0 ± 0.2 mJy in the 3 mm CARMA-15 data. We subtract the best-fit point source models from the visibility data sets before proceeding.

We next apply a phase shift to the CARMA-15 visibilities to establish a single phase center for all ten data sets. At this stage, all of the visibilities can be combined to form a single dirty map (Figure 3). However, this map is difficult to interpret because it includes data with dramatically different primary beams, and because noise at small angular scales masks the arcminute-scale emission. In order to proceed, we must use some image deconvolution method such as the Maximum Entropy Method (MEM) or CLEAN. For simplicity, we choose to build a model of the cluster iteratively using the CLEAN algorithm, though we note that MEM also holds promise for future work.

Our algorithm successively builds up a single model of the cluster in image space by CLEANing individual data sets. We begin by making a dirty map from the first data set $y_1(u, v)$. We then run the Högbom CLEAN algorithm (Högbom 1974) on this map with gain 0.05, stopping at 2.5σ . The CLEAN components are corrected for the appropriate primary beam, and a restored map is generated. This restored map (in units of Compton y per pixel) is our initial cluster model. The cluster model is then multiplied by the primary beam of the next data set, $y_2(u, v)$, and the result is Fourier transformed and subtracted from $y_2(u, v)$. From these model-subtracted visibilities, a dirty map is produced and Högbom CLEANed. The CLEAN components are corrected for the primary beam and restored, and the restored map is added to the cluster model. We repeat this process on all ten data sets, resulting in a cluster model that incorporates information from all of our data. We continue refining the model by making additional passes through all ten data sets until each model-subtracted dirty map is consistent with noise. Three iterations are found to be sufficient. Our final cluster model is then added to the weighted average of the ten model-subtracted dirty maps to form a CLEAN map (Figure 4). Though the resolution of the map is not well-defined, the smallest restoring beam of the ten used to construct the model is $10''.6 \times 16''.9$.

To assess the accuracy and flux recovery of our deconvolution technique, we construct a heuristic model of RX J1347.5–1145. We generate mock data using this model, repeat the procedure described above on the simulated visibilities, and compare the results to the input model. Modeling the SZ signal requires knowledge of the density n_e and the temperature T_e of the ICM, both of which can be approximated using the results of Allen et al. (2002) (hereafter A02) derived from *Chandra* X-ray data. For the electron density, we use the A02 density fit

within the central region with an $\alpha = -2.331$ power law in the outer region inferred from the A02 surface brightness profile fit. We piece together the inner and outer regions by requiring that $n_e(r)$ be continuous. For the electron temperature, we use the A02 measured temperature profile out to the outer radius of their largest bin, and use the average temperature of 12.0 keV at larger radii. We assign a temperature of 18.0 keV in the shocked region of the southeast quadrant. Finally, we truncate both the temperature and density profiles at r_{200} .

Using these approximations for the electron density and temperature, we integrate along the line of sight to produce a simulated Compton y map, and Fourier transform to produce simulated visibilities $y_{\text{sim}}(u, v)$. We then randomize the phases in our visibility data $y(u, v)$ to produce simulated noise $y_{\text{noise}}(u, v)$ and run our iterative CLEAN algorithm on $y_{\text{sim}}(u, v) + y_{\text{noise}}(u, v)$. We find that our algorithm accurately reproduces the morphology of the input model, and that it recovers 69%, 78%, and 92% of the integrated flux within r_{200} , r_{500} , and r_{2500} , where the r_{Δ} values are determined from the Allen et al. (2002) NFW model fit. The flux recovery ratio at larger radii is highly sensitive to the assumed electron density power law index. This is due to the fact that r_{200} for this cluster corresponds to an angular scale of $5''.75$, comparable to the $10''.7$ FWHM 3.5 m primary beam at 1 cm.

5. RESULTS

The map shown in Figure 4 can be understood as a relaxed cluster SZ signal with additional sub-arcminute structure in the southeast quadrant imparted by the merger event. The imaging of both the extended and compact structure in our SZ map is of significantly higher fidelity than previous measurements due to the ability of CARMA to remove the central point source and to the large angular dynamic range of the combined arrays. In contrast with previous work (Mason et al. 2010; Komatsu et al. 2000), we find that the peaks of the SZ and X-ray signals are coincident. Figure 6 shows a comparison between the CARMA SZ map and the *Chandra* X-ray pressure map (Bradač et al. 2008). Though a full multi-wavelength reconstruction is beyond the scope of this paper, it is obvious that the two techniques produce maps with consistent morphologies.

To separate the relaxed and disturbed components, we make use of the pressure profile fit to the *Chandra* X-ray data described in Allen et al. (2008), in which the southeast quadrant was excised. We first project the pressure profile along the line of sight to produce an integrated pressure map. For each sub-array, we multiply this map by the appropriate primary beam, convert to Compton y , Fourier transform, and subtract the result from the visibility data. We then iteratively build a model of the remaining SZ signal, following the procedure described in Section 4. We allow the X-ray pressure profile to be scaled by a multiplicative constant to compensate for cluster projection effects and calibration errors. The scale factor is chosen so as to produce no net CARMA-8 (arcminute-scale) signal in the iteratively-determined model.

Removing this estimate of the relaxed signal from our visibility data allows us to focus on the sub-arcminute-scale signal resulting from the merger event. The result

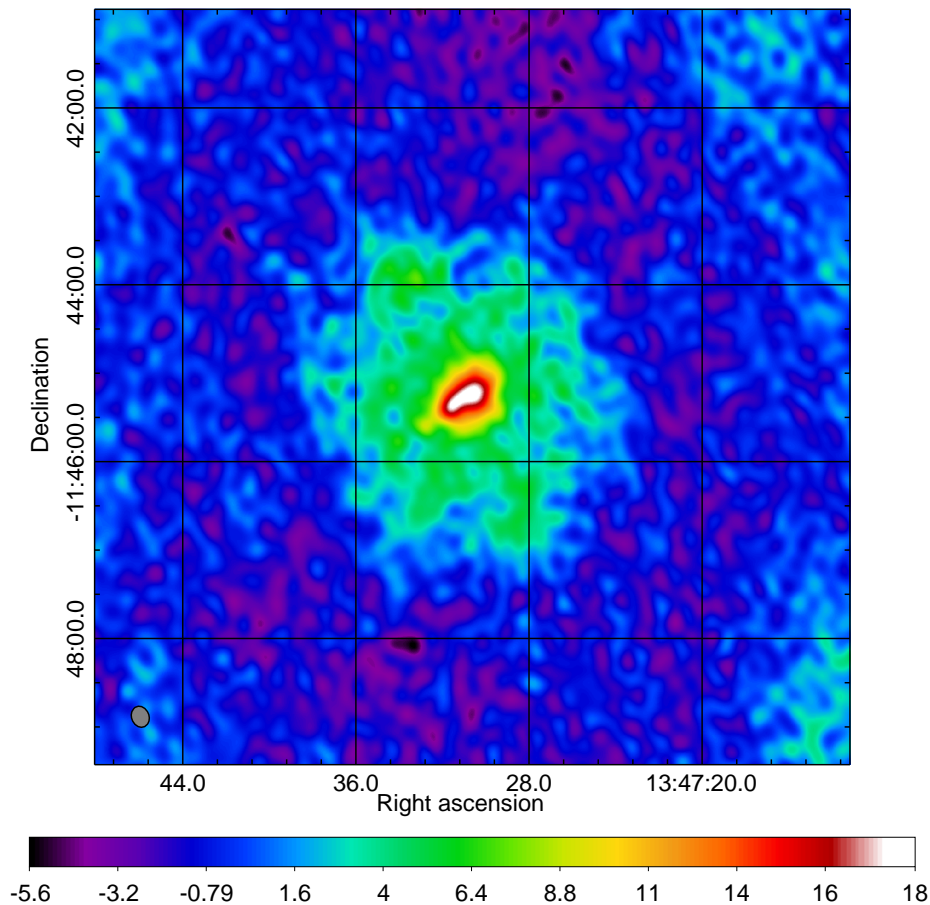


FIG. 3.— Dirty map of RX J1347.5–1145 using “robust” visibility weighting. The synthesized beam is shown in grey in the lower left. The map is in units of Compton $y \times 10^{13}/\text{beam}$.

is shown in Figure 5. The total Compton y signal recovered in this map, which corresponds to the fraction of the thermal energy in the cluster ICM associated with the merger-related substructure, is 9.1% of the total recovered from the map in Figure 4.

The value of the multiplicative constant by which the X-ray pressure is scaled can also yield information about the characteristics of the cluster. Since the scale factor is determined by requiring consistency with the CARMA-8 data, its value depends upon the three-dimensional morphology of the ICM on large angular scales. Due to the different dependencies of the X-ray surface brightness and the SZ signal on density, a cluster more (less) extended along the line of sight than in the plane of the sky would yield a scale factor of greater than (less than) one (see e.g., Grego et al. 2004). For this cluster, we find a scale factor of 0.58, indicating a cluster which is strongly compressed along the line-of-sight direction. A similar ratio is reported in Bonamente et al. (2011) using the CARMA-8 data reported here. Chakrabarty et al. (2008), using a combination of X-ray and SZ data, also find that RX J1347.5–1145 is compressed along the line of sight with an axis ratio of ~ 5 . A simple comparison of the X-ray surface brightness profile and our data, assuming an isothermal cluster, implies compression along the line of sight by a factor of roughly three-to-one—

a fairly extreme value, though less than suggested by Chakrabarty et al. (2008).

Clumping of the ICM, i.e., a systematic discrepancy between $\langle n_e^2(r) \rangle$ and $\langle n_e(r) \rangle^2$, could also lead to differences between the SZ and X-ray signals. Clumping is observed in the outskirts of simulated clusters (Nagai & Lau 2011), and is implied by observations of flattened entropy profiles and gas mass fractions apparently in excess of the cosmic mean in some clusters (e.g., Simionescu et al. 2011). However, in both cases the clumping occurs at large cluster radii (at least $> r_{500}$), and is thus unlikely to affect the normalization of the X-ray model used here (which was fit to data at $r < r_{500}$) at the level required to explain the offset.

The difference between the CARMA and *Chandra* pressure estimates could also arise in principle from calibration or systematic errors in the SZ or X-ray data. As a cross-check of our CARMA calibration, we compared our data to previous BIMA SZ measurements reported in Bonamente et al. (2008), finding consistent integrated Y values and binned visibility data. Since the *Chandra* calibration is unlikely to be mistaken at this level, and since major mergers such as RX J1347.5–1145 are not expected to be spherically symmetric, we suggest that line-of-sight compression is most likely to be the dominant effect. However, ICM clumping and calibration er-

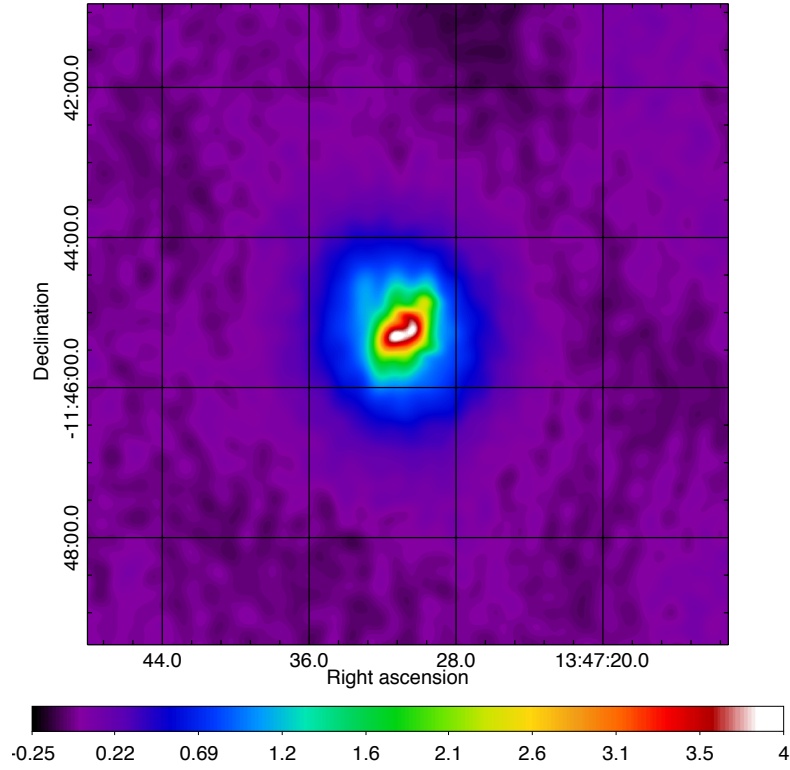


FIG. 4.— CLEAN map of RX J1347.5–1145. The map is in units of Compton $y \times 10^{15}$ /pixel, where the pixel size is $0.5'' \times 0.5''$. The smallest CLEAN beam used to construct the model is $10''.6 \times 16''.9$

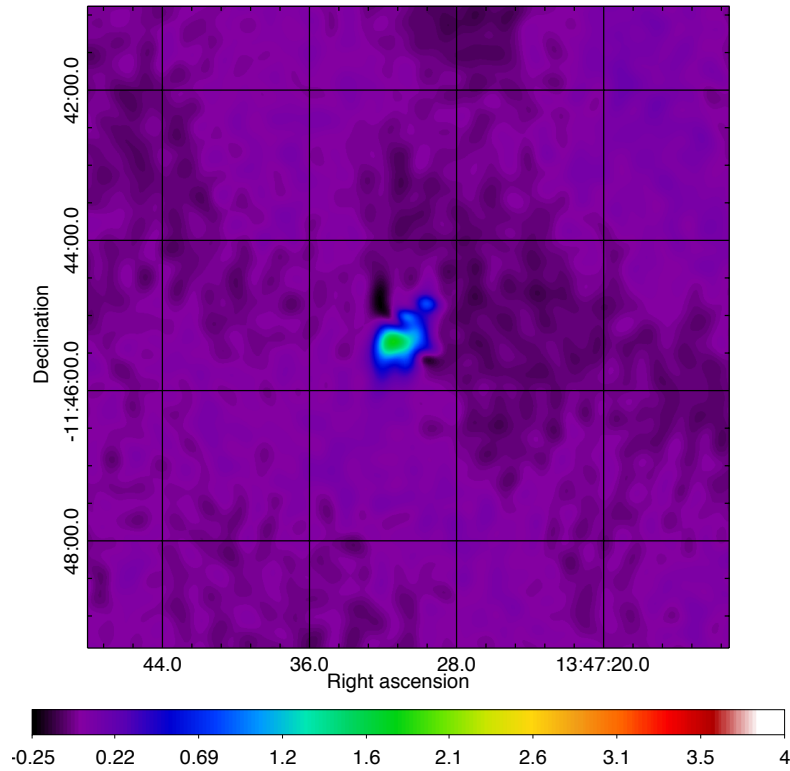


FIG. 5.— CLEAN map of RX J1347.5–1145 with the scaled relaxed X-ray pressure profile subtracted from the visibilities. The map is in units of Compton $y \times 10^{15}$ /pixel, where the pixel size is $0.5'' \times 0.5''$.

rors may also be contributing to the discrepancy; a more complete explanation will require a joint analysis of the two data sets.

6. CONCLUSIONS AND FUTURE WORK

We have demonstrated the ability of CARMA to measure the SZ signature of galaxy clusters at high sensitivity across a wide range of angular scales. By combining data from three CARMA configurations and two frequency bands, we measure the arcminute-scale SZ signal as well as the pressure substructure of RX J1347.5–1145. The large angular dynamic range of the CARMA data and the capability to constrain and remove point sources make our measurement a significant improvement in image fidelity over previous work (e.g., Korngut et al. 2011). By comparing our data to the X-ray measurements of Allen et al. (2008), we are able to determine that $\sim 9\%$ of the SZ signal is localized in the disturbed region of the cluster, and that the system is likely compressed along the line of sight relative to the plane of the sky.

Although our results demonstrate that CARMA in its current form is a highly capable SZ instrument, several upgrades will soon bring about significant enhancements. An effort is currently underway to equip all antennas with 1 cm receivers and expand the correlator bandwidth to 8 GHz for a 23-element array. The 3 mm CARMA-23 array described in this work provided sensitivity from uv radii of ~ 2.0 to $10k\lambda$; the upgraded array placed in the same configuration but operated at 1 cm will provide higher-sensitivity coverage from ~ 0.35 to $3.3k\lambda$. As shown in Figure 2, this corresponds to the portion of the uv plane where the SZ signal is large. A planned upgrade to more sensitive 3 mm receivers will allow the SZ signal at finer angular scales to be measured more precisely.

The sensitivity to smaller angular scale SZ structures provided CARMA's larger telescopes can be directed to-

ward regions of interest, as was done in this study by pointing them toward the region of hot gas to the southeast of the cluster center. With the increased sensitivity enabled by the ongoing upgrades, this technique can be used to search for shock-enhanced features in the outskirts of clusters. Mosaicking can also be used to provide sensitivity to small-scale structures over the entire cluster.

Taken together, these upgrades and observing strategies will allow CARMA to image clusters precisely and efficiently over a wide angular dynamic range, making it possible to fully exploit the power of the SZ effect as a probe of cluster astrophysics and precision cosmology.

ACKNOWLEDGEMENTS

We thank Evan Million for providing the X-ray pressure data from Bradač et al. (2008). We also thank Maruša Bradač and Myriam Gitti for useful discussions.

Support for CARMA construction was derived from the Gordon and Betty Moore Foundation, the Kenneth T. and Eileen L. Norris Foundation, the James S. McDonnell Foundation, the Associates of the California Institute of Technology, the University of Chicago, the states of California, Illinois, and Maryland, and the National Science Foundation. Ongoing CARMA development and operations are supported by the National Science Foundation under a cooperative agreement, including grant AST-0838187 at the University of Chicago, and by the CARMA partner universities. Partial support is provided by NSF Physics Frontier Center grant PHY-1125897 to the Kavli Institute of Cosmological Physics. D. P. M. was supported for part of this work by NASA through Hubble Fellowship grant HST-HF-51259.01.

Finally, we thank the CARMA staff for making the 23-element commissioning observations possible.

Facilities: CARMA

REFERENCES

- Allen, S. W., Rapetti, D. A., Schmidt, R. W., Ebeling, H., Morris, R. G., & Fabian, A. C. 2008, *MNRAS*, 383, 879, 0706.0033
- Allen, S. W., Schmidt, R. W., & Fabian, A. C. 2002, *MNRAS*, 335, 256, arXiv:astro-ph/0111368
- Bonamente, M. et al. 2011, *ArXiv e-prints*, 1112.1599
- Bonamente, M., Joy, M., LaRoque, S. J., Carlstrom, J. E., Nagai, D., & Marrone, D. P. 2008, *ApJ*, 675, 106
- Bradač, M. et al. 2008, *ApJ*, 681, 187, 0711.4850
- Carlstrom, J. E., Holder, G. P., & Reese, E. D. 2002, *ARA&A*, 40, 643
- Chakrabarty, D., de Filippis, E., & Russell, H. 2008, *A&A*, 487, 75
- Condon, J. J., Cotton, W. D., Greisen, E. W., Yin, Q. F., Perley, R. A., Taylor, G. B., & Broderick, J. J. 1998, *AJ*, 115, 1693
- Gitti, M., Ferrari, C., Domainko, W., Feretti, L., & Schindler, S. 2007, *A&A*, 470, L25, 0706.3000
- Gitti, M., & Schindler, S. 2004, *A&A*, 427, L9, arXiv:astro-ph/0409627
- Grego, L., Vrtilik, J. M., Van Speybroeck, L., David, L. P., Forman, W., Carlstrom, J. E., Reese, E. D., & Joy, M. K. 2004, *ApJ*, 608, 731, arXiv:astro-ph/0402139
- Högbom, J. A. 1974, *A&AS*, 15, 417
- Kitayama, T., Komatsu, E., Ota, N., Kuwabara, T., Suto, Y., Yoshikawa, K., Hattori, M., & Matsuo, H. 2004, *PASJ*, 56, 17, arXiv:astro-ph/0311574
- Komatsu, E., Matsuo, H., Kitayama, T., Hattori, M., Kawabe, R., Kohno, K., Kuno, N., & Suto, Y. 2000, *PASJ* – submitted: astro-ph/0006293
- Korngut, P. M. et al. 2011, *ApJ*, 734, 10, 1010.5494
- Malu, S. S., Subrahmanyan, R., Wieringa, M., & Narasimha, D. 2010, *ArXiv e-prints*, 1005.1394
- Mason, B. S. et al. 2010, *ApJ*, 716, 739
- Miranda, M., Sereno, M., de Filippis, E., & Paolillo, M. 2008, *MNRAS*, 385, 511, 0801.1429
- Muchovej, S., et al. 2007, *ApJ*, 663, 708
- Nagai, D., & Lau, E. T. 2011, *ApJ*, 731, L10, 1103.0280
- Rudy, D. J. 1987, PhD thesis, California Institute of Technology, Pasadena.
- Sault, R. J., Teuben, P. J., & Wright, M. C. H. 1995, in *Astronomical Society of the Pacific Conference Series*, Vol. 77, *Astronomical Data Analysis Software and Systems IV*, ed. R. A. Shaw, H. E. Payne, & J. J. E. Hayes, 433, arXiv:astro-ph/0612759
- Simionescu, A. et al. 2011, *Science*, 331, 1576, 1102.2429
- Voges, W. et al. 1999, *A&A*, 349, 389, arXiv:astro-ph/9909315
- Zemcov, M. et al. 2012, *ArXiv e-prints*, 1202.0029

TABLE 1
CARMA OBSERVATIONS OF RX J1347.5–1145.

Array	Ant 1	Ant 2	Frequency (GHz)	uv cutoff ($k\lambda$)	Noise mJy/beam	Minor axis arcsec	Major axis arcsec	Beam P.A. Degrees
CARMA-8	3.5m	3.5m	31	2000	0.16	100.1	128.8	-33.4
CARMA-15	10.4m	10.4m	90	10000	0.38	13.4	16.8	72.9
CARMA-15	10.4m	6.1m	90	10000	0.19	12.8	16.5	-44.8
CARMA-15	6.1m	6.1m	90	10000	0.30	15.1	37.4	3.0
CARMA-23	10.4m	10.4m	86	10000	0.22	13.9	14.6	-80.2
CARMA-23	10.4m	6.1m	86	10000	0.14	14.4	16.4	-65.3
CARMA-23	6.1m	6.1m	86	10000	0.26	14.9	37.3	4.4
CARMA-23	10.4m	3.5m	88	10000	0.80	16.2	18.3	59.1
CARMA-23	6.1m	3.5m	88	10000	0.76	10.6	16.9	-81.1
CARMA-23	3.5m	3.5m	88	5000	2.64	31.4	67.5	-44.3

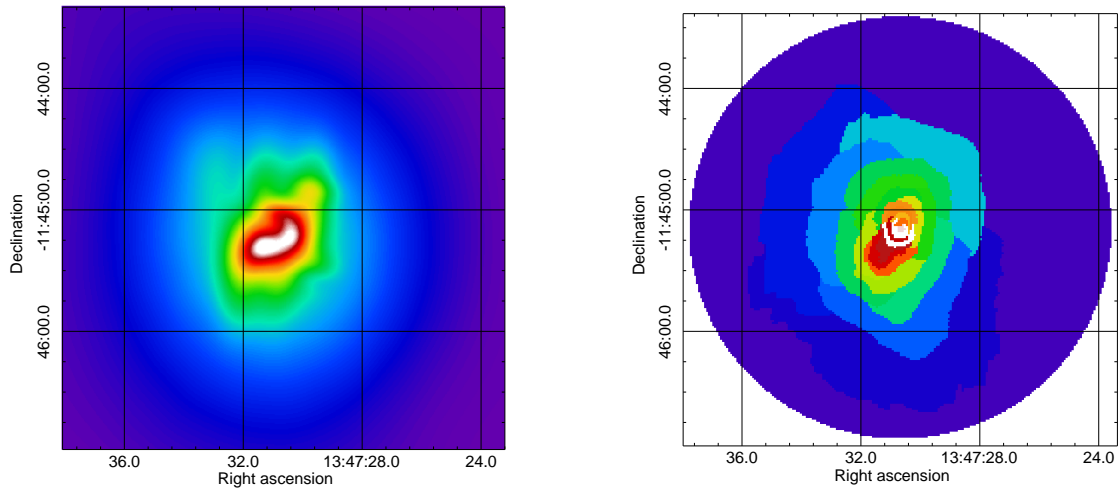


FIG. 6.— The CLEANed CARMA SZ map (left) cropped and scaled for direct comparison with the published X-ray-derived integrated pressure map from Bradač et al. (2008) (right).